chinaXiv:201705.00533v1

Silicon Oxycarbide/Carbon Nanohybrids with Tiny Silicon Oxycarbide Particles Embedded in Free Carbon Matrix Based on Photoactive Dental Methacrylates

Meimei Wang,[†,‡] Yonggao Xia,[†] Xiaoyan Wang,[†,§] Ying Xiao,[†] Rui Liu,[∥] Qiang Wu,[⊥] Bao Qiu,[†] Ezzeldin Metwalli,[#] Senlin Xia,[#] Yuan Yao,[#] Guoxin Chen,[†] Yan Liu,[†] Zhaoping Liu,[†] Jian-Qiang Meng,[§] Zhaohui Yang,[⊥] Ling-Dong Sun,[∥] Chun-Hua Yan,[∥] Peter Müller-Buschbaum,[#] Jing Pan,[‡] and Ya-Jun Cheng*[,†]

[†]Ningbo Institute of Materials Technology and Engineering, Chinese Academy of Sciences, 1219 Zhongguan West Road, Zhenhai District, Ningbo, Zhejiang Province 315201, People's Republic of China

[‡]Faculty of Materials Science and Chemical Engineering, Ningbo University, Ningbo, Zhejiang Province 315211, People's Republic of China

[§]State Key Laboratory of Separation Membranes and Membrane Processes, Tianjin Polytechnic University, Tianjin 300387, People's Republic of China

[∥]Beijing National Laboratory for Molecular Sciences, State Key Laboratory of Rare Earth Materials Chemistry and Applications and PKU-HKU Joint Lab on Rare Earth Materials and Bioinorganic Chemistry, College of Chemistry and Molecular Engineering, Peking University, Beijing 100871, People's Republic of China

[⊥]Center for Soft Condensed Matter Physics and Interdisciplinary Research, Soochow University, Suzhou 215006, People's Republic of China

[#]Physik-Department, Lehrstuhl für Funktionelle Materialien, Technische Universität München, James-Franck-Strasse 1, 85748 Garching, Germany

Supporting Information

ABSTRACT: A new facile scalable method has been developed to synthesize silicon oxycarbide (SiOC)/carbon nanohybrids using difunctional dental methacrylate monomers as solvent and carbon source and the silane coupling agent as the precursor for SiOC. The content (from 100% to 40% by mass) and structure (ratio of disordered carbon over ordered carbon) of the free carbon matrix have been systematically tuned by varying the mass ratio of methacryloxypropyltrimethoxysilane (MPTMS) over the total mass of the resin monomers from 0.0 to 6.0. Compared to the bare carbon anode, the introduction of MPTMS significantly improves the electrochemical performance as a lithium-ion battery anode. The initial and cycled discharge/charge capacities of the SiOC/C nanohybrid anodes reach maximum with the MPTMS ratio of 0.50, which displays very good rate performance as well. Detailed structures and electrochemical performance as lithium-ion battery anodes have been systematically investigated. The structure−property correlation and corresponding mechanism have been discussed.

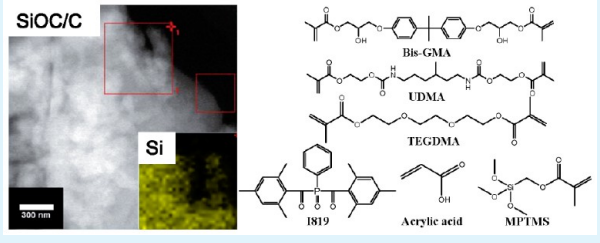

KEYWORDS: *silane coupling agent, thermosetting methacrylate resin, silicon oxycarbide, lithium-ion battery anode, photopolymerization*

INTRODUCTION

Lithium-ion batteries (LIBs) are widely used as an energy supply of electric vehicles, hybrid electric vehicles, portable electronic devices, and energy storage as well because of their high energy density, long cycling life, minimum memory effect, and environmental benignity.[1−6] However, the conventional graphite anode cannot meet the continuous increasing technical standard due to low capacity (372 mAh·g^{-1}) and serious safety concerns.[6−8] It is crucial to develop a new generation of lithium-ion battery anodes with high specific capacity, excellent cyclic stability, good rate performance, and reliable operation safety.

Polymer-derived ceramics (PDCs) such as silicon oxycarbide (SiOC) have attracted much attention as a potential LIB anode material.[9−21] They have advantages such as large capacity, good cyclic stability, and potential low costs. Moreover, they can be easily synthesized.[17] In more detail, SiOC glass contains Si−C and Si−O bonds and its chemical composition can be defined as SiO_xC_{4-x} + yC_{free}.[22] In this notation, the term SiO_xC_{4-x}

chinaXiv:201705.00533v1

denotes the "pure" silicon oxycarbide glass and the term C_{free} represents the additional free carbon within the material.[11,23,24] This free carbon is important for the electrochemical performance because it acts as major active sites for lithium ion intercalation.[25] It is reported that the Li ions are stored both in the interspaces of the sheetlike carbon and at the edges of the graphene layers.[25] The Si−O−C network mainly functions as stabilizer to inhibit electrode collapse during repeated discharge/charge progresses.[26] The composition, structure, morphology of the SiOC glass and free carbon matrix, and homogeneous dispersion of the SiOC glass within the free carbon matrix play important roles in the overall performance of the SiOC composites.[27−30] In particular, it was reported that composites with the SiOC glass homogeneously dispersed in free carbon matrix tend to exhibit better electrochemical device performance.[27,28,30] Therefore, the current research on SiOC lithium-ion battery anodes has been mainly focused on the carbon-rich SiOC composites, where continuous free carbon is formed and used as matrix to disperse the SiOC glass.[25−28,31−36]

In most literature, SiOC was synthesized by pyrolysis of linear polysiloxanes.[11,15,16,37−43] However, because the thermoplastic polysiloxanes are molten during pyrolysis, the nucleation, growth, and aggregation of the in situ formed SiOC domain structure is only poorly controlled. As a result, large-sized bulk SiOC glasses were formed.[23] Such large-size structures are not beneficial for the structure stability and overall electrochemical performance of the SiOC composites. Furthermore, the pyrolysis of the thermoplastic linear polysiloxanes generates only rather limited content of free carbon. Consequently, only nanosized carbon domain could be formed, leading to a segregated SiOC glass and carbon phase.[30] To overcome these problems, photo or thermal cross-linking treatment was applied to the linear polysiloxanes to improve the structure and morphology control of the SiOC and carbon phase during pyrolysis.[15,17,21,24,27,28,34,39,44−49] Unfortunately, the enhanced cross-linking alone did not bring sufficient structure and morphology control due to a limited number of cross-linking sites, which resulted in only a moderate electrochemical performance improvement. In literature, further optimization of the pyrolysis protocol was reported with the aim of tuning the structure and performance of the SiOC composites.[26−28,31,32,34,50]

In the present manuscript a novel way toward a more optimized structure and morphology control of SiOC/C nanohybrids is presented. It is based on our previous work that enabled the homogeneous dispersion of tiny SiOC particles in a continuous free carbon matrix.[51−53] To our best knowledge, this synthetic method was only rarely applied before.[54] As shown in Scheme 1, unlike the typically exploited linear and/or cross-linking modified polymeric siloxane precursors, a polymerizable silane coupling agent (methacryloxypropyltrimethoxysilane, MPTMS) is utilized as the source for siloxane in our route. Moreover, difunctional methacrylate monomers (bisphenol A glycerolate methacrylate, Bis-GMA, urethane dimethacrylate, UDMA, and triethylene glycol dimethacrylate, TEGDMA) are used as reaction medium and carbon source as well.[51,52] The silane coupling agent is homogeneously premixed with the methacrylate monomers at the molecular level. Additionally, acrylic acid (AA) is used as additional cross-linker to further enhance the integration of the MPTMS with the difunctional methacrylate network, because AA reacts with the triple methoxyl silane groups of MPTMS to significantly increase the number of the cross-linking units of the MPTMS. Furthermore, photopolymerization triggered by a visible light active initiator (phenylbis(2,4,6-trimethylbenzoyl)phosphine oxide, I819) is performed. Upon photopolymerization, the cross-linked polymer reaches its gel point within 1 min and the liquid monomer solution is converted to a solid almost instantaneously. The photopolymerization has advantages compared with conventional thermally initiated polymerization, because the fast solidification process effectively inhibits the phase separation between the silane and methacrylate network during polymerization.[54] Due to the above-mentioned

Scheme 1. SiOC/C Nanohybrid Fabrication and Molecular Structures of the Methacrylate Resin Monomers, Silane Coupling Agent, and Photoinitiator Used in the Synthesis of the SiOC/C Nanohybrids

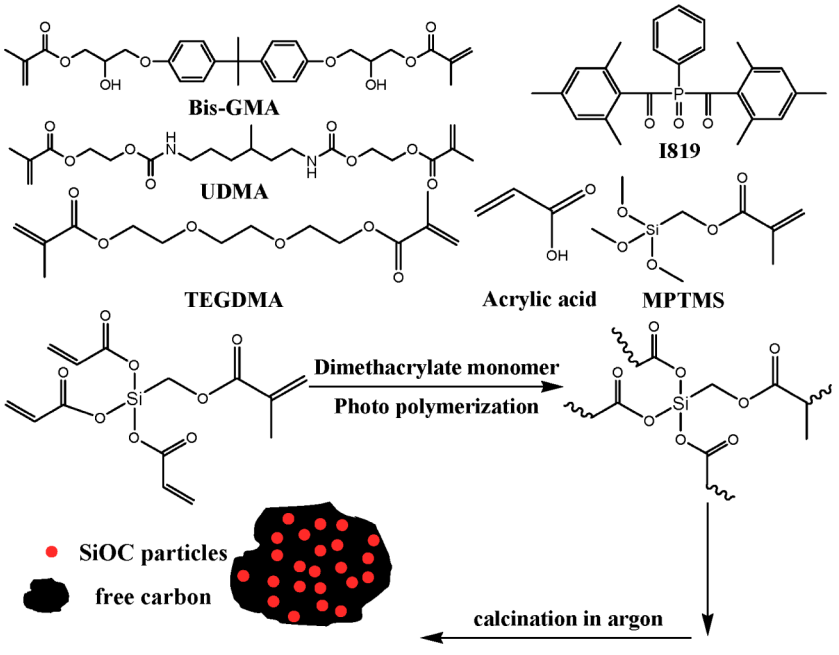

reasons, the copolymerization between the silane coupling agent and methacrylate monomers generates highly cross-linked thermosetting polysiloxanes. The silane molecules are well-mixed and integrated with the thermosetting methacrylate network at a molecular level. Compared to the pristine linear or cross-linking modified linear polysiloxanes, the pyrolysis of the highly cross-linked polysiloxanes exercises better structure and morphology control of the SiOC glass and the free carbon matrix. The melting process of the thermosetting methacrylate is significantly inhibited during calcination in argon. As a result, the nucleation, growth, and agglomeration of the SiOC glass are effectively inhibited. Thus, the original structure of the MPTMS within the methacrylate network is well-replicated in the final SiOC composite. Besides the benefit of structure and morphology control, the strategy developed in the present work is also featured with a fact that the tedious, costly, and environmentally unfriendly waste solvent disposal process is totally circumvented because all of the solution components are converted to solids via polymerization.

EXPERIMENTAL SECTION

Materials. Acrylic acid (AA, 99%) and *N*-methylpyrrolidone (NMP, 98.0%) were purchased from Sinopharm Group Co., Ltd. Bis-GMA, UDMA, TEGDMA were donated by Esstech, Inc., U.S.A. Phenylbis-(2,4,6-trimethylbenzoyl)phosphine oxide (Irgacure 819 photoinitiator, I819, 97%) was purchased from Sigma-Aldrich. Methacryloxypropyltrimethoxysilane (MPTMS, 97%) was purchased from Aladdin. Poly(vinylidene fluoride) (PVDF) was donated by Solvay. Conductive carbon black (Super P, 99% on metals basis) was purchased from Alfa Aesar.

Sample Preparation. First, Bis-GMA, UDMA, and TEGDMA were mixed together with a mass ratio of 4:6:4. Photoactive B/U/T resin mixture was prepared by dissolving I-819 (1% mass fraction) into the solution. MPTMS (from 0 to 12.0 g) was further mixed with 2.0 g of the B/U/T solution and 2.0 g of AA, with continuous stirring for around 5 min. The as-prepared solution was poured into a silicone rubber mold which was clamped between two glass slides afterward. Photopolymerization was carried out with a visible light-curing unit (Luxomat D, blue light 9 W, range of emission: 350−500 nm) for 3 min each side. The solidified samples were further baked at 60 °C in an oven for 24 h. The samples were cut into powders by a mixer after being released from the molds. Calcination in argon atmosphere was performed at 800 °C for 4 h in tube furnace with a ramp rate of 5 K/min starting from room temperature, followed by natural cooling to room temperature. Then, the calcined samples were ball-milled by a planetary ball miller (FRITSCH-pulverizette 7, Germany) for 4 h with the speed of 400 rpm, followed by sieving with a 300 mesh.

Sample Characterization. Field emission scanning electron microscopy (FESEM) images were obtained with a Hitachi S4800 scanning electron microscope (Tokyo, Japan) at an accelerating voltage of 4 kV. The transmission electron microscopy (TEM) experiment was performed with a JEOL JEM-2100F TEM or Tecnai F20 (America FEI) instrument operated at 200 kV. FESEM EDX elemental mapping was carried out with an FEI QUANTA 250 FEG (America FEI) at an accelerating voltage of 15 kV. X-ray diffraction (XRD) was carried out with 2θ ranging between 5° and 90° (Bruker AXS D8 Advance, λ = 1.541 Å, 2.2 kW). The carbon content of the samples were determined by a

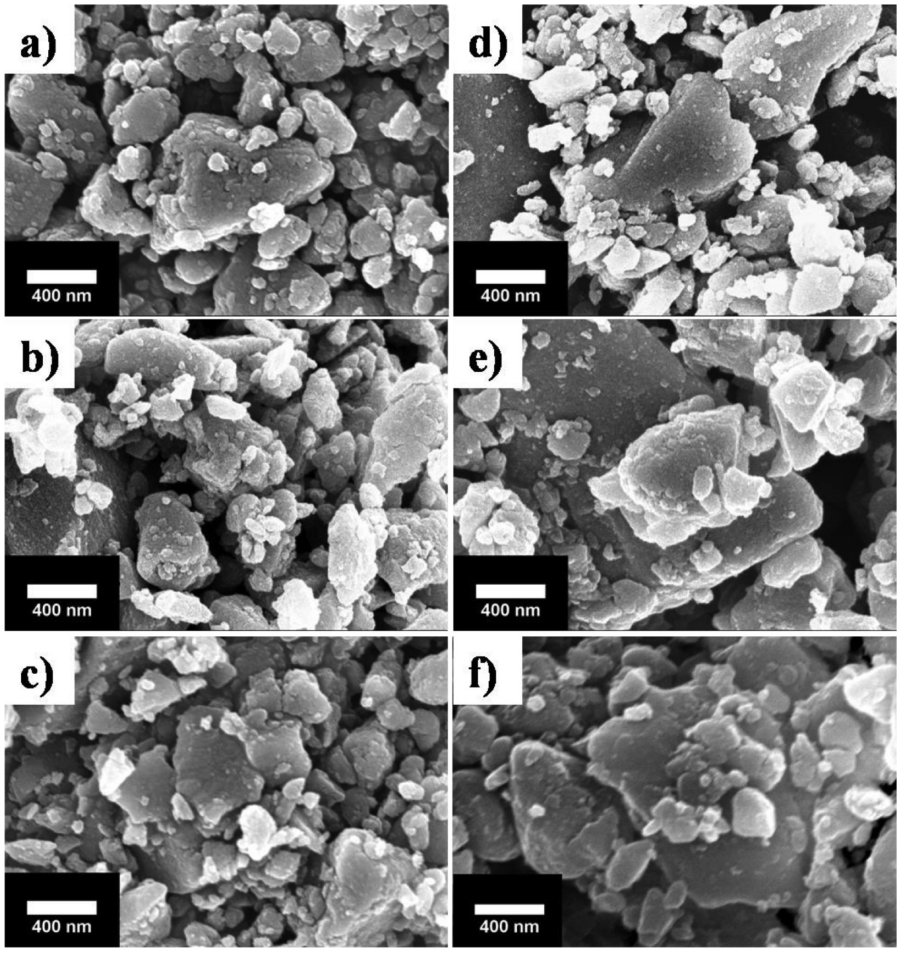

Figure 1. SEM images of the SiOC/C nanohybrids prepared with different mass ratios of MPTMS over the total mass of the methacrylate resins at high magnification: (a) 0, (b) 0.125, (c) 0.25, (d) 0.50, (e) 1.0, and (f) 6.0.

chinaXiv:201705.00533v1

chinaXiv:201705.00533v1

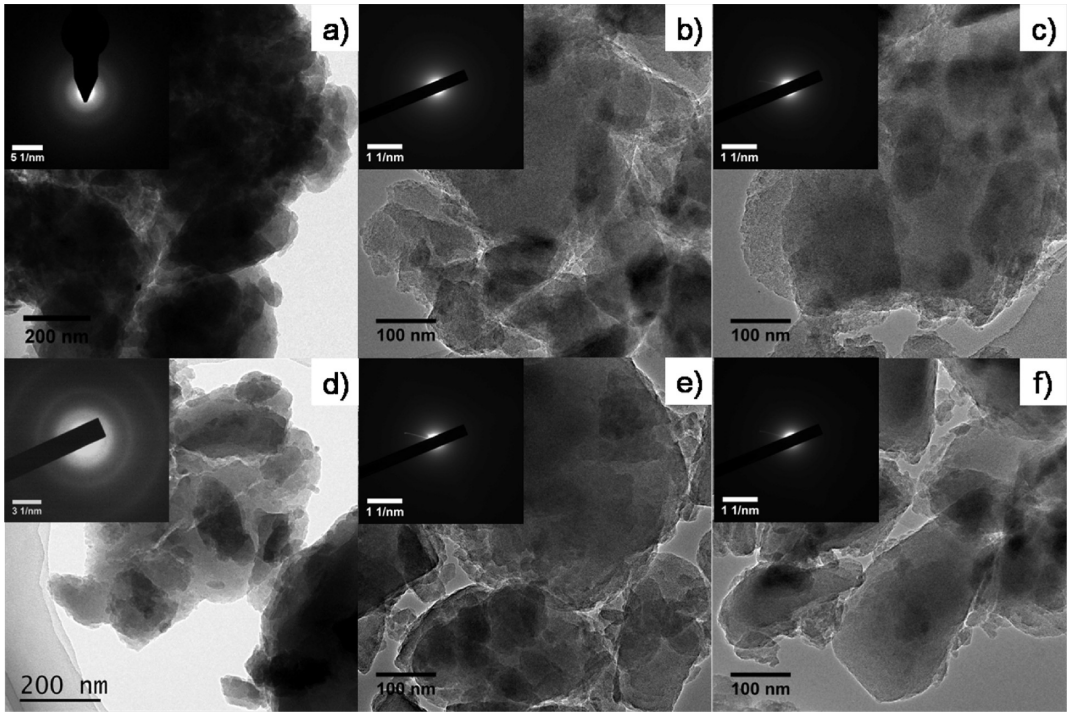

Figure 2. TEM images of the SiOC/C nanohybrids prepared with different mass ratios of MPTMS over the total mass of the methacrylate resins: (a) 0, (b) 0.125, (c) 0.25, (d) 0.50, (e) 1.0, and (f) 6.0. Inset: SAED pattern of each TEM image.

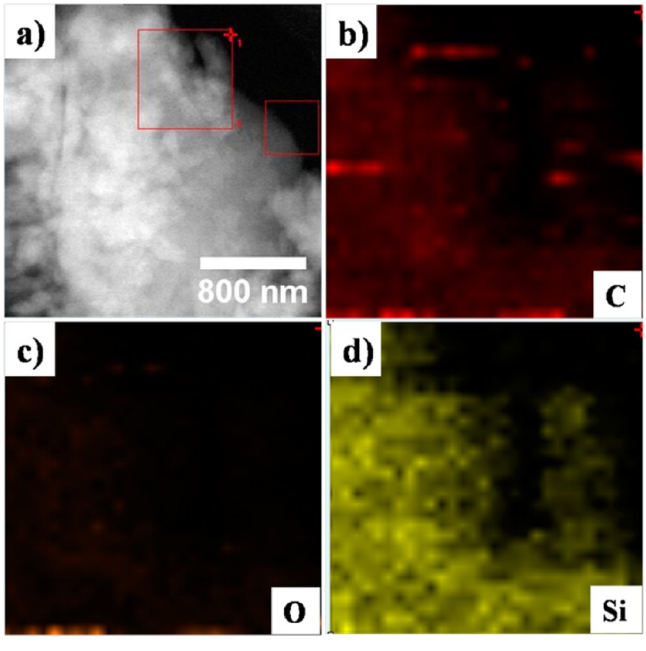

Figure 3. STEM images of the SiOC/C nanohybrid prepared with the mass ratio of MPTMS over the total mass of the methacrylate resin of 0.50: (a) TEM image; elemental mapping of (b) carbon, (c) oxygen, and (d) silicon. The box 1 (in image a) was used as position reference, and the smaller box was used for mapping.

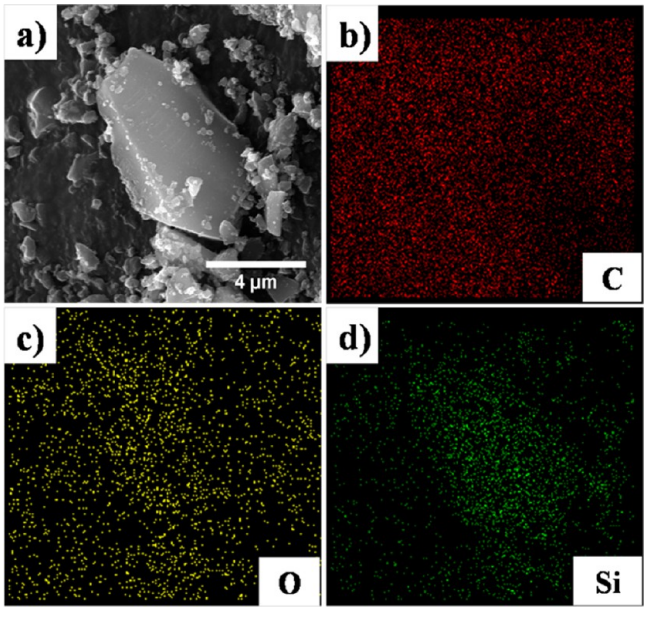

Figure 4. EDX images of the SiOC/C nanohybrid prepared with the mass ratio of MPTMS over the total mass of the methacrylate resin of 0.50: (a) SEM image; elemental mapping of (b) carbon, (c) oxygen, and (d) silicon.

thermogravimetric analyzer (TGA, Mettler Toledo, Switzerland) in air with the temperature range defined between 50 and 800 °C and the ramp rate set at 20 K/min. Raman spectroscopy was collected on a Renishaw (in Via-reflex) with the excitation wavelength of 532 nm. X-ray photoelectron spectroscopy (XPS) measurement was done with an ESCALAB 250Xi spectrometer, using focused monochromatized Al Kα radiation ($h\nu$ = 1486.6 eV) at room temperature. The oxygen and carbon contents of the samples were determined by O/N analyzer (EMGA-620W, Japan) and high-frequency infrared carbon sulfur analyzer (CS844, LECO). The content of silicon was derived by subtracting the total contents of carbon and oxygen. Before elemental analysis, the samples were dried in vacuum oven at 80 °C overnight. Small-angle X-ray scattering (SAXS) measurements were performed using a Ganesha 300XL SAXS–WAXS system (SAXS LAB ApS, Copenhagen/Denmark) with an X-ray wavelength of 0.154 nm (Cu anode). The detector was positioned at a distance of 1051 mm from the sample. Glass capillaries were used as sample containers for the SAXS measurements.

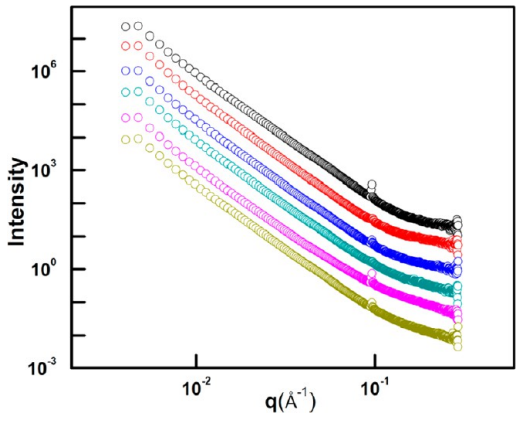

Figure 5. SAXS of the SiOC/C nanohybrids prepared with different mass ratios of MPTMS over the total mass of the methacrylate monomers: black, 0; red, 0.125; blue, 0.25; dark cyan, 0.50; magenta, 1.0; dark yellow, 6.0.

Electrochemical Measurement. 2032-type coin cell devices were fabricated to evaluate the electrochemical performance of the SiOC/C nanohybrids. A slurry mixture was prepared by dispersing the active material, Super P and PVDF (mass ratio: 8:1:1) in NMP. Thereafter, the slurry mixture was spread on a piece of copper foil by doctor blading, followed by drying at 80 °C in vacuum for 12 h. After the copper foil was pressed and punched into round discs with a diameter of 13 mm, the discs were dried in over at 80 °C in oven further for 4 h.

The half-cell was fabricated using lithium foil as the counter electrode. The mass loading density for the active material was more than 1 mg/cm^2. Electrolyte from Dongguan Shanshan Battery Material Co., Ltd. was used, where 1.0 M $LiPF_6$ was dissolved in a mixture of ethylene carbonate (EC) and diethyl carbonate (DMC) (1:2 v/v). The volume of the electrolyte applied was around 100 μL. The rate performance was measured at the current density sequence of 0.1, 0.2, 0.5, 1.0, 2.0, 5.0, 10, 20, and 0.1 C in the voltage range between 3.0 and 0.005 V (vs Li/Li$^+$) (five cycles each current density, 1 C = 500 mA·g^{-1}). The cyclic measurement was carried out at a current density of 0.2 C in the voltage range of 3.0−0.005 V (vs Li/Li$^+$) for 50 rounds. The specific capacity was calculated based on the mass of the active material. The lithiation process was defined as discharge process, and the corresponding delithiation process was defined as charge process. Cyclic voltammetry (CV) test was performed on a CHI 1040B potentiostat/galvanostat analyzer (Shanghai Chenhua instrument Co., Ltd.) with a scanning rate of 0.1 mV/s in the range between 0.005 and 3 V.

RESULTS AND DISCUSSION

Morphology of the SiOC/C Nanohybrids. SEM images of the SiOC/C nanohybrids prepared with different amounts of MPTMS are shown in Figure 1. Particles with a broad size distribution are observed, which are confirmed by the low-magnification SEM images as shown in Figure S1. Because with SEM it is hard to distinguish the SiOC nanoparticles within the nanohybrid, TEM is further applied to uncover the structure details of the nanohybrids. However, still no distinct morphologies can be observed with TEM with different mass ratios of MPTMS over the total mass of the methacrylate resins (from 0 to 6.0) (Figure 2). Thus, it is assumed that SiOC particles with very small size are homogeneously dispersed in the carbon matrix. This assumption is partially confirmed by scanning transmission electron microscopy (STEM) images (Figure 3), where the elements of silicon, oxygen, and carbon are homogeneously distributed in a region with the dimension of 300 nm × 300 nm. It is true that the mapping signal of carbon also contains the contribution from the carbon matrix. However, the mapping signal of silicon and oxygen indicates that SiOC is homogeneously embedded in the carbon matrix at the molecular level. As a complementary method, energy-dispersive X-ray spectroscopy (EDX) shows that SiOC is well-dispersed in the area of the carbon matrix with a large size scale (10 μm × 10 μm) (Figure 4). Moreover, one needs to consider that the spatial resolution of EDX is much lower than the size of SiOC. However, by combing the SEM, TEM, STEM, and EDX data, it is reasonable to say that SiOC with very small size is homogeneously embedded in the carbon matrix at different length scales. The featureless selected area electron diffraction (SAED) patterns of the TEM images

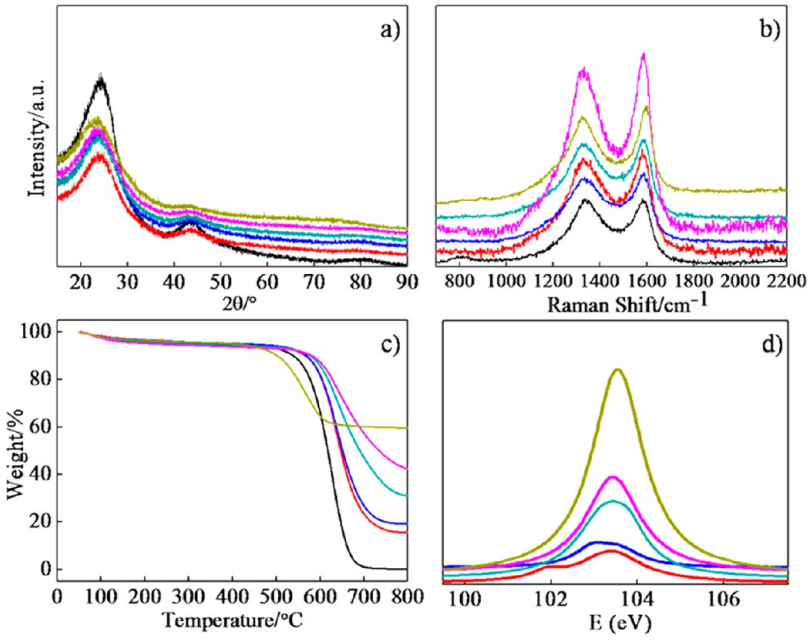

Figure 6. TGA (a), XRD (b), Raman (c), and XPS (d) of the SiOC/C nanohybrids prepared with different mass ratios of MPTMS over the total mass of the methacrylate resin monomers: black, 0; red, 0.125; blue, 0.25; dark cyan, 0.50; magenta, 1.0; dark yellow, 6.0.

chinaXiv:201705.00533v1

Table 1. Elemental Composition and Chemical Formula of the SiOC Nanohybrids

MPTMS mass ratio	silicon %	oxygen % of SiOC glass	carbon %	chemical formula
0.125	4.3	8.2	79.4	$SiO_{3.43}C_{0.53}$ + 42.63C_{free}
0.25	7.5	12.7	72.4	$SiO_{2.95}C_{1.05}$ + 21.47C_{free}
0.50	12.5	21.0	60.3	$SiO_{2.91}C_{1.09}$ + 10.12C_{free}
1.0	15.9	26.4	52.4	$SiO_{2.89}C_{1.11}$ + 6.59C_{free}
6.0	30.5	36.3	29.9	$SiO_{2.10}C_{1.90}$ + 0.11C_{free}

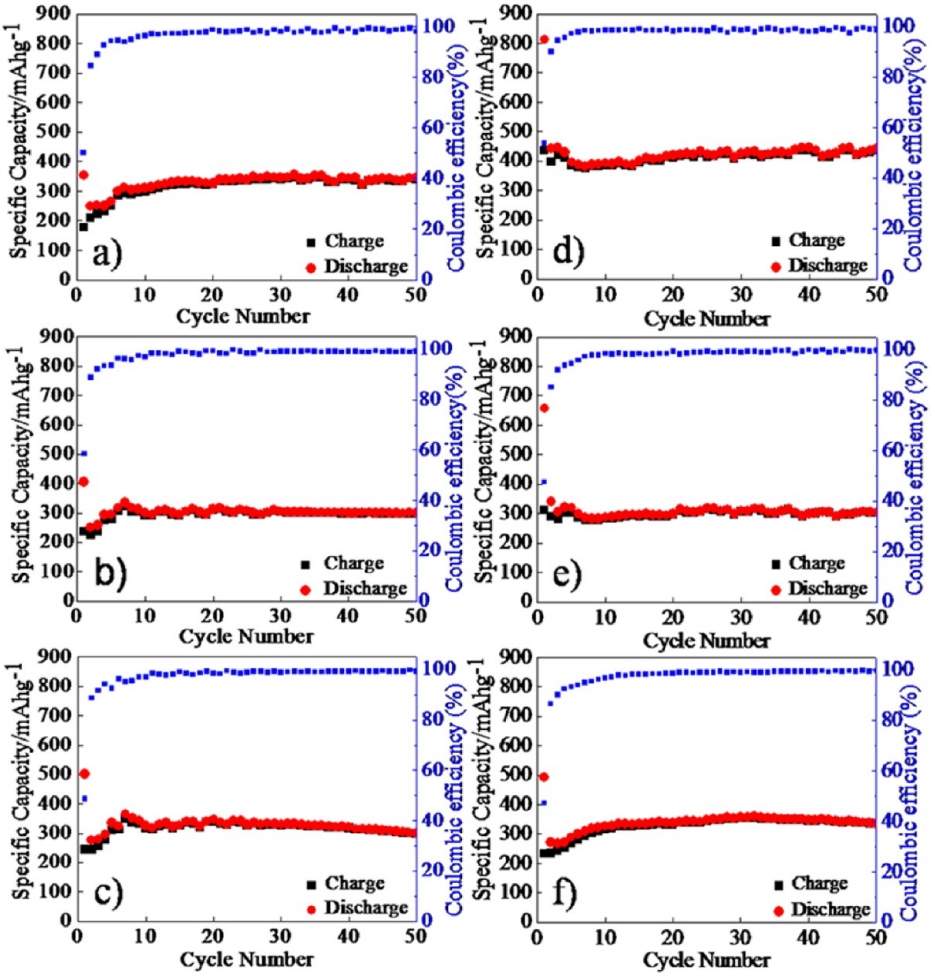

Figure 7. Cyclic performance of the SiOC/C nanohybrids prepared with different mass ratios of MPTMS over the total mass of the methacrylate resins: (a) 0, (b) 0.125, (c) 0.25, (d) 0.50, (e) 1.0, and (f) 6.0.

(inset in Figure 2) suggest that both SiOC and carbon matrix are amorphous in nature.

Besides the imaging analysis in local areas, the average statistic structure information on the SiOC/C nanohybrids is investigated by SAXS. According to Figure 5, very small particles with the size of around 2 nm exist in the nanohybrids and no characteristic nanostructures in the range of 5−200 nm are observed. As a consequence, the SAXS data confirm the assumption about the sample morphology gained from the TEM and STEM image analysis.

Composition of the SiOC/C Nanohybrids. With the mass ratio of MPTMS over the total mass of the resin monomer systematically varied at 0, 0.125, 0.25, 0.50, 1.0, and 6.0, the amount of the free carbon matrix is decreased from 100% to 84%, 80%, 69%, 58%, and 40%, respectively (Figure 6a, TGA). An exponential correlation between the free carbon matrix content and the mass ratio of MPTMS is exhibited (Figure S2). Because the mass ratio of MPTMS is varied in an exponential style, the observed exponential decrease of free carbon content indicates that the specific carbon yield does not change significantly regarding the individual mass ratio of MPTMS. The XRD patterns of the SiOC/C nanohybrids with different amounts of carbon are shown in Figure 6b. Only two broad peaks at 23.9° and 43.0° are observed, which are ascribed to the local graphitized carbon structures within the amorphous carbon phase.[27] Because the graphitic signal is very weak, the free carbon is supposed to be mainly amorphous. No further diffraction peaks are observed, which again suggests that the SiOC is amorphous. The nature of the carbon phase is further analyzed with Raman spectroscopy (Figure 6c). Two peaks located at 1360 and 1580 cm^{-1} are ascribed to disordered carbon (D band) and graphitized carbon (G band), respectively.[29,55,56] Integral intensities of the D-band and G-band within each spectrum are obtained by Lorentzian fit. In all spectra the intensities of the D band are larger than those of the G band, suggesting that the disordered carbon is excess than the ordered carbon.[26] The bare carbon

chinaXiv:201705.00533v1

chinaXiv:201705.00533v1

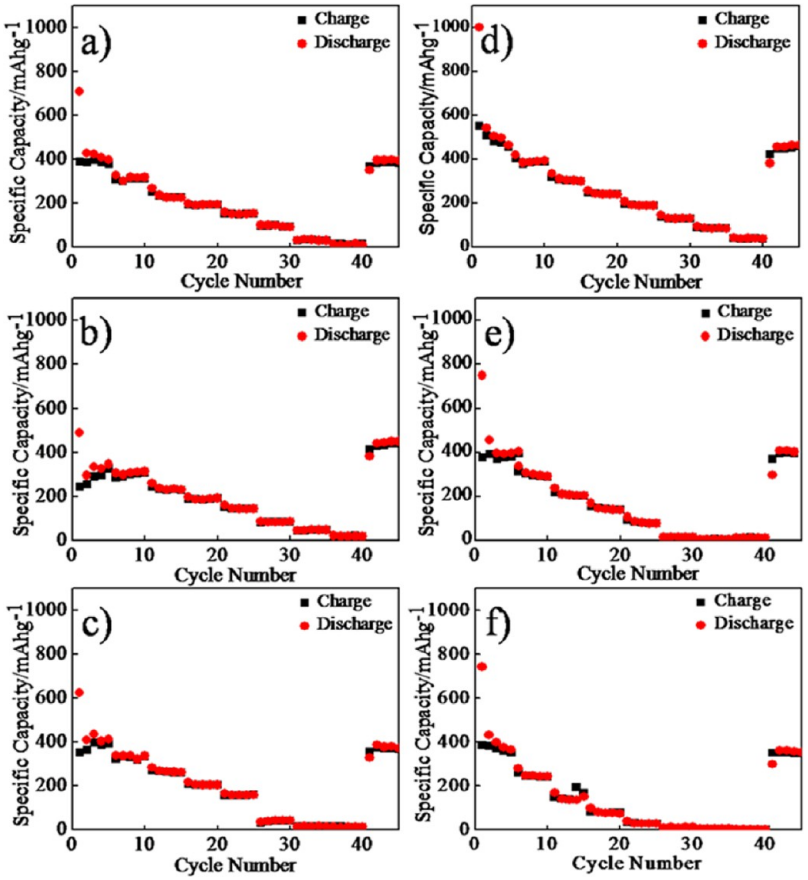

Figure 8. Rate performance of the SiOC/C nanohybrids prepared with different mass ratios of MPTMS over the total mass of the methacrylate resins: (a) 0, (b) 0.125, (c) 0.25, (d) 0.50, (e) 1.0, and (f) 6.0. The rate performance was conducted by five cycles at each current density of 0.1, 0.2, 0.5, 1.0, 2.0, 5.0, 10, 20, and 0.1 C (1 C = 500 $mA{\cdot}g^{-1}$).

sample has the smallest D band peak width and lowest intensity ratio of $I(D)/I(G)$ compared to those SiOC/C nanohybrids. This indicates that the bare carbon sample has the least amount of disordered carbon. With the introduction of MPTMS, the D band peak width and intensity ratio of $I(D)/I(G)$ continue to increase until the mass ratio of MPTMS reaches 0.50, followed by inverse decrease with further increasing mass ratio of MPTMS to 6.0. The results suggest that a small amount of MPTMS promotes the formation of disordered carbon, whereas large mass ratio of MPTMS reduces the amount of disordered carbon. With the introduction of MPTMS into the resin mixture, the methoxylsilane functional group tends to react with the hydroxyl group of Bis-GMA and/or AA to form the Si−O− group due to the effect of entropy increase. As a result, the silane molecule acts as a cross-linking center to enhance the overall cross-linking degree of the methacrylates. However, simultaneously, the methacrylate group of the MPTMS copolymerizes with the difunctional methacrylates. Due to the monofunctional nature of the MPTMS, the copolymerization will reduce the cross-linking degree of the methacrylate network. Therefore, with a small amount of MPTMS, the cross-linking enhanced by the reaction between silane and hydroxyl group dominates because each MPTMS has three methoxyl silane functional groups. As a result, the formation of disordered carbon is promoted. When the amount of MPTMS is increased, the reaction between silane and hydroxyl group tends to be saturated. Nevertheless, the copolymerization between methacrylate group of MPTMS and resin monomer is continuously enhanced, leading to decreased cross-linking degree and reduced formation of disordered carbon.[27]

In order to explore the local bonding state of the silicon atom, XPS was conducted. AS shown in Figure 6d, the shoulder peak located at about 102 eV indicates the existence of SiO_2C_2, whereas the main peaks at about 103 eV are typical for other types of Si−O bonds.[24] With increasing amount of MPTMS, the main peaks shift toward a higher bonding energy value that is typical for the silicon atom bonded to oxygen.[57] Besides, the intensity of the shoulder peak gradually diminishes until almost invisible. It implies continuous increasing oxygen content within nanohybrids with increasing amount of MPTMS.

Elemental analysis is performed to further investigate the chemical composition of the SiOC/C nanohybrids. The elemental analysis of the bare carbon sample indicates the existence of 10.18% oxygen within the carbon matrix. On the basis of this fact, the actual oxygen content belonging to the SiOC glass is obtained by abstracting the total oxygen content obtained from elemental analysis with the oxygen content in the free carbon matrix. The chemical formulas of the SiOC glass are derived according to the structure model of SiO_xC_{4-x}. Thereafter, the amount of the free carbon is calculated. As shown in Table 1, the contents of silicon and oxygen gradually increase along with increasing mass ratio of MPTMS, while the carbon content decreases significantly along with increasing mass ratio of MPTMS. It is consistent with the results reported by Bujalski et al.[58] The increased mass ratio of MPTMS decreases the relative mass ratio of the methacrylate resin monomers, which are supposed to be the main source for carbon content.

Electrochemical Performance of the SiOC/C Nanohybrids. The cyclic performance of the SiOC/C nanohybrid

anode at 0.2 C (100 mA·g^{-1}) between 0.005 and 3 V was tested for 50 cycles as shown in Figure 7. Regarding the bare carbon anode, the initial discharge/charge capacity is 675 and 357 mAh·g^{-1}, respectively, which are reduced to around 318 mAh·g^{-1} after 50 cycles. Several general trends can be summarized from the cyclic profiles of the SiOC/C nanohybrids. First, the initial discharge/charge capacities are increased with the mass ratio of MPTMS increased from 0.125 to 0.50, followed by inverse decrease with further increasing mass ratio of MPTMS from 0.50 to 6.0. In details, the discharge capacities are first increased from 405 to 813 mAh·g^{-1}, followed by decrease to 492 mAh·g^{-1}. Correspondingly, the charge capacities are increased from 237 to 436 mAh·g^{-1}, and then decreased to 232 mAh·g^{-1}. Second, after 50 cycles, the SiOC/C nanohybrids prepared with different mass ratios of MPTMS possess the discharge/charge capacities above 300 mAh·g^{-1}. Particularly, the highest capacity of 443 mAh·g^{-1} is achieved with the MPTMS mass ratio of 0.50, which is 40% better than the capacity of the bare carbon anode. It is found that the initial discharge/charge capacity of the bare carbon anode is higher than most of the SiOC/C nanohybrids except the one prepared with the MPTMS mass ratio of 0.50. It is reported that the SiOC is electrochemically inactive for lithiation and it mainly acts as a stabilizer for the carbon matrix.[29] Correspondingly, the free carbon matrix is considered as the major lithium storage site.[27] Therefore, introduction of SiOC into carbon matrix will reduce the overall capacity to some extent. This is one of the major reasons why the bare carbon anode exhibits higher capacities than most of the SiOC/C nanohybrids. However, from structure analysis, it is found that the increasing mass ratio of MPTMS generates more disordered carbon within the carbon matrix, which stores more lithium ions than typical graphitic (ordered) carbon. As a result, the overall capacity will be lifted by the formation of more disordered carbon. Particularly, the ratio of disordered carbon over ordered carbon reaches maximum with the MPTMS mass ratio of 0.50. This is the reason why the SiOC/C nanohybrid prepared with the MPTMS mass ratio of 0.50 exhibits the highest initial discharge/charge capacity and cyclic performance as well.

The rate performance was measured at the current densities ranging from 0.1 C (50 mA·g^{-1}) to 20 C (10 000 mA·g^{-1}). With the MPTMS mass ratio of 0.50, the largest capacities among all of the samples at each individual current density are observed (Figure 8). Compared to previously reported work, the rate performance of the sample is very good.[21] With a current density of 1000 mA·g^{-1} (5 C) the reversible capacities reach 140 mAh·g^{-1}. When the current densities further increase to 10 and 20 C, capacities of 90 and 40 mAh·g^{-1} are still retained, while the bare carbon anode exhibits only capacities close to zero at the same current density.

Compared to the previously reported work, the capacities can still be recovered to 470 mAh·g^{-1} at 0.1 C after cycles at high current density. It further shows good cyclic stability of the SiOC/C nanohybrid anode. The rate performance is related to nature of carbon matrix. As addressed previously, the SiOC/C

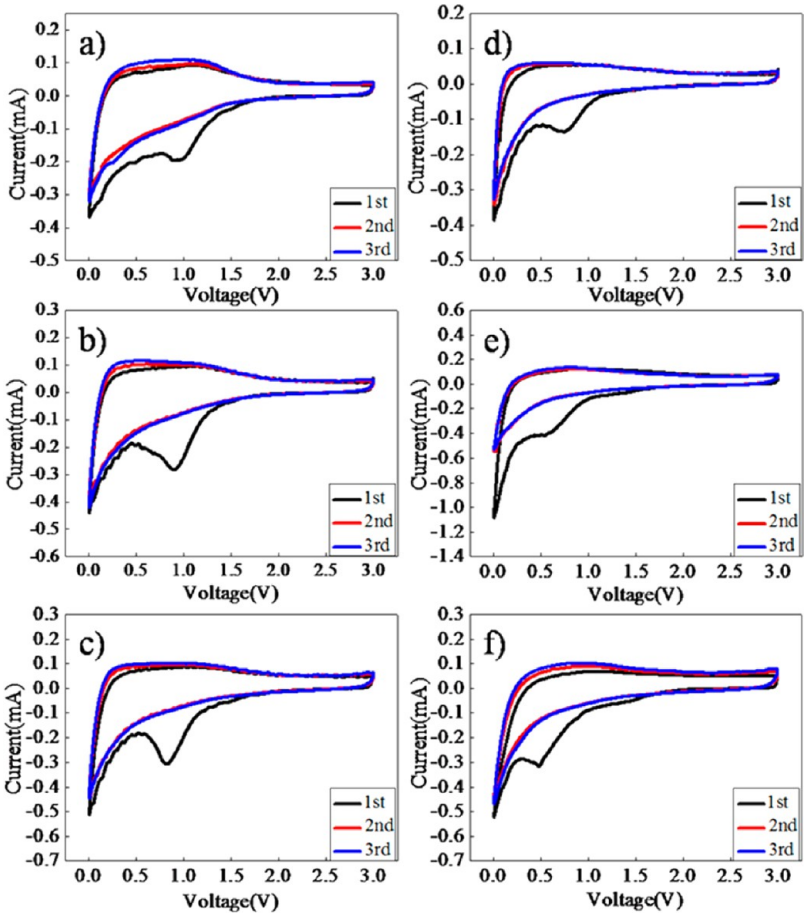

Figure 9. CV curves of the SiOC/C nanohybrids prepared with different mass ratios of MPTMS over the total mass of the methacrylate resins: (a) 0, (b) 0.125, (c) 0.25, (d) 0.50, (e) 1.0, and (f) 6.0.

chinaXiv:201705.00533v1

nanohybrid exhibits the highest ratio of disordered carbon over ordered carbon. It is commonly accepted that the disordered carbon possesses less electron conductivity than the ordered carbon, which will normally sacrifice the capacity under high current density. However, the disordered carbon offers higher capacity than the ordered carbon. Therefore, it can be concluded that a good balance between capacity and electron conductivity is achieved with the MPTMS mass ratio of 0.50, leading to the best rate performance.

Finally, the cyclic voltammetry profiles of the SiOC/C nanohybrids with different mass ratios of MPTMS are exhibited in Figure 9. The formation of a solid electrolyte interface (SEI) in the first cycle is confirmed by the peaks between 0.5 and 1 V. However, from the second cycle, no obvious peaks are observed, which is typical for the lithiation/delithiation process of carbon-based lithium-ion battery anode. The CV results confirm that the free carbon matrix plays a major active role in the electrochemical process.

CONCLUSION

A facile scalable method has been developed to synthesize SiOC/C nanohybrids with the free carbon content systematically varied between 100% and 40%. Small SiOC particles with the size around 2 nm are homogeneously embedded in carbon matrix as suggested by imaging and scattering techniques. The Raman spectroscopy reveals that the ratio of disordered carbon over ordered carbon is increased with the MPTMS mass ratio increased from 0 to 0.50, followed by inverse decrease with further increased mass ratio of MPTMS from 0.50 to 6.0. The change of the disordered/ordered carbon ratio is supposed to be the impact of the cross-linking degree modification of the methacrylate network brought by MPTMS. Correspondingly, the best electrochemical performance is achieved with the MPTMS mass ratio of 0.50. Compared to bare carbon anode, both, the initial discharge and charge capacities are significantly increased at the current density of 100 $mA{\cdot}g^{-1}$ (813 vs 675 $mAh{\cdot}g^{-1}$ for discharge capacity, and 436 vs 357 $mAh{\cdot}g^{-1}$ for charge capacity). Moreover, the capacities after 50 cycles at 100 $mA{\cdot}g^{-1}$ are effectively improved by more than 40%, which reaches around 443 $mAh{\cdot}g^{-1}$. Particularly, an outstanding rate performance of the SiOC/C nanohybrid anode is observed compared to previously reported work. With the current density of 5000 $mA{\cdot}g^{-1}$ (10 C), the capacities are still retained at 90 $mAh{\cdot}g^{-1}$. After cycles at high current densities, the capacities can still be recovered to 470 $mAh{\cdot}g^{-1}$ at the current density of 50 $mA{\cdot}g^{-1}$. Besides the stabilization effect of the SiOC particles within the free carbon matrix, a good balance between high capacity contribution from disordered carbon and good electron conductivity from ordered carbon is supposed to be responsible for the very good rate performance. Further application of the SiOC/C nanohybrids in lithium-ion battery anode, for example, as a buffer medium for silicon nanoparticulate anode to improve the electrochemical performance, is in progress.[13]

ASSOCIATED CONTENT

Supporting Information

The Supporting Information is available free of charge on the ACS Publications website at DOI: 10.1021/acsami.6b05032.

Low-magnification SEM image and correlation profile between carbon matrix content and mass ratio of MPTMS (PDF)

AUTHOR INFORMATION

Corresponding Author

*E-mail: chengyj@nimte.ac.cn.

Notes

The authors declare no competing financial interest.

ACKNOWLEDGMENTS

This research is funded by the Natural Science Foundation of China (51103172), the Zhejiang Nonprofit Technology Applied Research Program (2013C33190), and the open project of the Beijing National Laboratory for Molecular Science (20140138), the CAS-EU S&T cooperation partner program (174433KYSB20150013), and Ningbo Key Laboratory of Polymer Materials. S.X. and Y.Y. acknowledge the China Scholarship Council (CSC), and P.M.-B. acknowledges funding by the Center for NanoScience (CeNS) Munich. Donation of the dental resins from Esstech Inc., U.S.A., is greatly appreciated.

REFERENCES

(1) Wen, Z. H.; Lu, G. H.; Mao, S.; Kim, H.; Cui, S. M.; Yu, K. H.; Huang, X. K.; Hurley, P. T.; Mao, O.; Chen, J. H. Silicon Nanotube Anode for Llithium-Ion Batteries. *Electrochem. Commun.* **2013**, *29*, 67–70.

(2) Tao, H. C.; Fan, L. Z.; Qu, X. H. Facile Synthesis of Ordered Porous Si@C Nanorods as Anode Materials for Li-Ion Batteries. *Electrochim. Acta* **2012**, *71*, 194–200.

(3) Guerfi, A.; Charest, P.; Dontigny, M.; Trottier, J.; Lagace, M.; Hovington, P.; Vijh, A.; Zaghib, K. SiOx-Graphite as Negative for High Energy Li-Ion Batteries. *J. Power Sources* **2011**, *196* (13), 5667–5673.

(4) Zhou, X. S.; Guo, Y. G. A PEO-assisted Electrospun Silicon-Graphene Composite as an Anode Material for Lithium-ion Batteries. *J. Mater. Chem. A* **2013**, *1* (32), 9019–9023.

(5) Zhou, M.; Cai, T. W.; Pu, F.; Chen, H.; Wang, Z.; Zhang, H. Y.; Guan, S. Y. Graphene/Carbon-Coated Si Nanoparticle Hybrids as High-Performance Anode Materials for Li-Ion Batteries. *ACS Appl. Mater. Interfaces* **2013**, *5* (8), 3449–3455.

(6) Hong, I.; Scrosati, B.; Croce, F. Mesoporous, Si/C Composite Anode for Li Battery Obtained by 'Magnesium-Thermal' Reduction Process. *Solid State Ionics* **2013**, *232*, 24–28.

(7) Wang, J.; Zhao, H. L.; He, J. C.; Wang, C. M.; Wang, J. Nano-Sized SiOx/C Composite Anode for Lithium Ion Batteries. *J. Power Sources* **2011**, *196* (10), 4811–4815.

(8) Xue, L. G.; Xu, G. J.; Li, Y.; Li, S. L.; Fu, K.; Shi, Q.; Zhang, X. W. Carbon-Coated Si Nanoparticles Dispersed in Carbon Nanotube Networks As Anode Material for Lithium-Ion Batteries. *ACS Appl. Mater. Interfaces* **2013**, *5* (1), 21–25.

(9) Shen, J.; Ahn, D.; Raj, R. C-Rate Performance of Silicon Oxycarbide Anodes for Li Plus Batteries Enhanced by Carbon nanotubes. *J. Power Sources* **2011**, *196* (5), 2875–2878.

(10) Graczyk-Zajac, M.; Fasel, C.; Riedel, R. Polymer-Derived-SiCN Ceramic/Graphite Composite as Anode Material with Enhanced Rate Capability for Lithium Ion Batteries. *J. Power Sources* **2011**, *196* (15), 6412–6418.

(11) Mera, G.; Navrotsky, A.; Sen, S.; Kleebe, H.-J.; Riedel, R. Polymer-Derived SiCN and SiOC Ceramics - Structure and Energetics at the Nanoscale. *J. Mater. Chem. A* **2013**, *1* (12), 3826–3836.

(12) Nara, H.; Yokoshima, T.; Momma, T.; Osaka, T. Highly Durable SiOC Composite Anode Prepared by Electrodeposition for Lithium Secondary Batteries. *Energy Environ. Sci.* **2012**, *5* (4), 6500–6505.

(13) Choi, S.; Jung, D. S.; Choi, J. W. Scalable Fracture-Free SiOC Glass Coating for Robust Silicon Nanoparticle Anodes in Lithium Secondary Batteries. *Nano Lett.* **2014**, *14* (12), 7120–7125.

chinaXiv:201705.00533v1

chinaXiv:201705.00533v1

(14) Xing, W. B.; Wilson, A. M.; Eguchi, K.; Zank, G.; Dahn, J. R. Pyrolyzed Polysiloxanes for Use as Anode Materials in Lithium-Ion Batteries. *J. Electrochem. Soc.* **1997**, *144* (7), 2410−2416.
(15) Wilson, A. M.; Zank, G.; Eguchi, K.; Xing, W.; Dahn, J. R. Pyrolysed Silicon-Containing Polymers as High Capacity Anodes for Lithium-Ion Batteries. *J. Power Sources* **1997**, *68* (2), 195−200.
(16) Colombo, P.; Mera, G.; Riedel, R.; Soraru, G. D. Polymer-Derived Ceramics: 40 Years of Research and Innovation in Advanced Ceramics. *J. Am. Ceram. Soc.* **2010**, *93* (7), 1805−1837.
(17) Ahn, D.; Raj, R. Cyclic Stability and C-Rate Performance of Amorphous Silicon and Carbon Based Anodes for Electrochemical Storage of Lithium. *J. Power Sources* **2011**, *196* (4), 2179−2186.
(18) Li, Y.; Hu, Y.; Lu, Y.; Zhang, S.; Xu, G.; Fu, K.; Li, S.; Chen, C.; Zhou, L.; Xia, X.; Zhang, X. One-Dimensional SiOC/C Composite Nanofibers as Binder-Free Anodes for Lithium-Ion Batteries. *J. Power Sources* **2014**, *254*, 33−38.
(19) Shen, J.; Raj, R. Silicon-Oxycarbide Based Thin Film Anodes for Lithium Ion Batteries. *J. Power Sources* **2011**, *196* (14), 5945−5950.
(20) Ahn, D.; Raj, R. Thermodynamic Measurements Pertaining to the Hysteretic Intercalation of Lithium in Polymer-Derived Silicon Oxycarbide. *J. Power Sources* **2010**, *195* (12), 3900−3906.
(21) Pradeep, V. S.; Graczyk-Zajac, M.; Riedel, R.; Soraru, G. D. New Insights in to the Lithium Storage Mechanism in Polymer Derived SiOC Anode Materials. *Electrochim. Acta* **2014**, *119*, 78−85.
(22) Saha, A.; Raj, R.; Williamson, D. L. A Model for the Nanodomains in Polymer-Derived SiCO. *J. Am. Ceram. Soc.* **2006**, *89* (7), 2188−2195.
(23) Tamayo, A.; Rubio, J.; Pena-Alonso, R.; Rubio, F.; Oteo, J. L. Gradient Pore Size Distributions in Porous Silicon Oxycarbide Materials. *J. Eur. Ceram. Soc.* **2008**, *28* (9), 1871−1879.
(24) Corriu, R. J. P.; Leclercq, D.; Mutin, P. H.; Vioux, A. Preparation and Structure of Silicon Oxycarbide Glasses Derived from Polysiloxane Precursors. *J. Sol-Gel Sci. Technol.* **1997**, *8* (1−3), 327−330.
(25) Dibandjo, P.; Graczyk-Zajac, M.; Riedel, R.; Pradeep, V. S.; Soraru, G. D. Lithium Insertion into Dense and Porous Carbon-Rich Polymer-Derived SiOC Ceramics. *J. Eur. Ceram. Soc.* **2012**, *32* (10), 2495−2503.
(26) Kaspar, J.; Graczyk-Zajac, M.; Riedel, R. Lithium Insertion into Carbon-Rich SiOC Ceramics: Influence of Pyrolysis Temperature on Electrochemical Properties. *J. Power Sources* **2013**, *244*, 450−455.
(27) Graczyk-Zajac, M.; Toma, L.; Fasel, C.; Riedel, R. Carbon-Rich SiOC Anodes for Lithium-Ion Batteries: Part I. Influence of Material UV-Pre-Treatment on High Power Properties. *Solid State Ionics* **2012**, *225*, 522−526.
(28) Kaspar, J.; Graczyk-Zajac, M.; Riedel, R. Carbon-Rich SiOC Anodes for Lithium-Ion Batteries: Part II. Role of Thermal Cross-Linking. *Solid State Ionics* **2012**, *225*, 527−531.
(29) Wilamowska, M.; Pradeep, V. S.; Graczyk-Zajac, M.; Riedel, R.; Soraru, G. D. Tailoring of SiOC Composition as a Way to Better Performing Anodes for Li-Ion Batteries. *Solid State Ionics* **2014**, *260*, 94−100.
(30) Liao, N. B.; Zheng, B. R.; Zhou, H. M.; Xue, W. Effect of Carbon Content on the Structure and Electronic Properties of Silicon Oxycarbide Anodes for Lithium-Ion Batteries: a First-Principles Study. *J. Mater. Chem. A* **2015**, *3* (9), 5067−5071.
(31) Soraru, G. D.; Pena-Alonso, R.; Kleebe, H.-J. The Effect of Annealing at 1400 Degrees C on the Structural Evolution of Porous C-Rich Silicon (boron)Oxycarbide Glass. *J. Eur. Ceram. Soc.* **2012**, *32* (8), 1751−1757.
(32) Pradeep, V. S.; Graczyk-Zajac, M.; Wilamowska, M.; Riedel, R.; Soraru, G. D. Influence of Pyrolysis Atmosphere on the Lithium Storage Properties of Carbon-Rich Polymer Derived SiOC Ceramic Anodes. *Solid State Ionics* **2014**, *262*, 22−24.
(33) Fukui, H.; Harimoto, Y.; Akasaka, M.; Eguchi, K. Lithium Species in Electrochemically Lithiated and Delithiated Silicon Oxycarbides. *ACS Appl. Mater. Interfaces* **2014**, *6* (15), 12827−12836.
(34) Kleebe, H.-J.; Blum, Y. D. SiOC Ceramic with High Excess Free Carbon. *J. Eur. Ceram. Soc.* **2008**, *28* (5), 1037−1042.
(35) Blum, Y. D.; MacQueen, D. B.; Kleebe, H. J. Synthesis and Characterization of Carbon-Enriched Silicon Oxycarbides. *J. Eur. Ceram. Soc.* **2005**, *25* (2−3), 143−149.
(36) Kaspar, J.; Graczyk-Zajac, M.; Riedel, R. Determination of the Chemical Diffusion Coefficient of Li-Ions in Carbon-Rich Silicon Oxycarbide Anodes by Electro-Analytical Methods. *Electrochim. Acta* **2014**, *115*, 665−670.
(37) Zhang, H.; Pantano, C. G. Synthesis and Characterization of Silicon Oxycarbide Glasses. *J. Am. Ceram. Soc.* **1990**, *73* (4), 958−963.
(38) Burns, G. T.; Taylor, R. B.; Xu, Y. R.; Zangvil, A.; Zank, G. A. High-Temperature Chemistry of the Conversion of Siloxanes to Silicon-carbide. *Chem. Mater.* **1992**, *4* (6), 1313−1323.
(39) Dibandjo, P.; Dire, S.; Babonneau, F.; Soraru, G. D. Influence of the Polymer Architecture on the High Temperature Behavior of SiCO Glasses: a Comparison between Linear- and Cyclic-Derived Precursors. *J. Non-Cryst. Solids* **2010**, *356* (3), 132−140.
(40) Fukui, H.; Ohsuka, H.; Hino, T.; Kanamura, K. Polysilane/Acenaphthylene Blends Toward Si-O-C Composite Anodes for Rechargeable Lithium-Ion Batteries. *J. Electrochem. Soc.* **2011**, *158* (5), A550−A555.
(41) Fukui, H.; Ohsuka, H.; Hino, T.; Kanamura, K. Preparation of Microporous Si-O-C Composite Material and Its Lithium Storage Capability. *Chem. Lett.* **2009**, *38* (1), 86−87.
(42) Su, D.; Li, Y.-L.; An, H.-J.; Liu, X.; Hou, F.; Li, J.-Y.; Fu, X. Pyrolytic Transformation of Liquid Precursors to Shaped Bulk Ceramics. *J. Eur. Ceram. Soc.* **2010**, *30* (6), 1503−1511.
(43) Larcher, D.; Mudalige, C.; George, A. E.; Porter, V.; Gharghouri, M.; Dahn, J. R. Si-Containing Disordered Carbons Prepared by Pyrolysis of Pitch Polysilane Blends: Effect of Oxygen and Sulfur. *Solid State Ionics* **1999**, *122* (1−4), 71−83.
(44) Sorarù, G. D.; Modena, S.; Guadagnino, E.; Colombo, P.; Egan, J.; Pantano, C. Chemical Durability of Silicon Oxycarbide Glasses. *J. Am. Ceram. Soc.* **2002**, *85* (6), 1529−1536.
(45) Fukui, H.; Ohsuka, H.; Hino, T.; Kanamura, K. Influence of Polystyrene/Phenyl Substituents in Precursors on Microstructures of Si-O-C Composite Anodes for Lithium-Ion Batteries. *J. Power Sources* **2011**, *196* (1), 371−378.
(46) Soraru, G. D.; Dalcanale, F.; Campostrini, R.; Gaston, A.; Blum, Y.; Carturan, S.; Aravind, P. R. Novel Polysiloxane and Polycarbosilane Aerogels via Hydrosilylation of Preceramic Polymers. *J. Mater. Chem.* **2012**, *22* (16), 7676−7680.
(47) Martinez-Crespiera, S.; Ionescu, E.; Kleebe, H.-J.; Riedel, R. Pressureless Synthesis of Fully Dense and Crack-Free SiOC Bulk Ceramics via Photo-Crosslinking and Pyrolysis of a Polysiloxane. *J. Eur. Ceram. Soc.* **2011**, *31* (5), 913−919.
(48) Xing, W. B.; Wilson, A. M.; Zank, G.; Dahn, J. R. Pyrolysed Pitch-Polysilane Blends for Use as Anode Materials in Lithium Ion Batteries. *Solid State Ionics* **1997**, *93* (3−4), 239−244.
(49) Wilson, A. M.; Xing, W. B.; Zank, G.; Yates, B.; Dahn, J. R. Pyrolysed Pitch-Polysilane Blends for Use as Anode Materials in Lithium Ion Batteries the Effect of Oxygen. *Solid State Ionics* **1997**, *100* (3−4), 259−266.
(50) Das, G.; Bettotti, P.; Ferraioli, L.; Raj, R.; Mariotto, G.; Pavesi, L.; Soraru, G. D. Study of the Pyrolysis Process of an Hybrid CH3SiO1.5 Gel into a SiCO Glass. *Vib. Spectrosc.* **2007**, *45* (1), 61−68.
(51) Wang, X.; Meng, J.-Q.; Wang, M.; Xiao, Y.; Liu, R.; Xia, Y.; Yao, Y.; Metwalli, E.; Zhang, Q.; Qiu, B.; Liu, Z.; Pan, J.; Sun, L.-D.; Yan, C.-H.; Mueller-Buschbaum, P.; Cheng, Y.-J. Facile Scalable Synthesis of TiO2/Carbon Nanohybrids with Ultrasmall TiO2 Nanoparticles Homogeneously Embedded in Carbon Matrix. *ACS Appl. Mater. Interfaces* **2015**, *7* (43), 24247−24255.
(52) Xiao, Y.; Wang, X.; Xia, Y.; Yao, Y.; Metwalli, E.; Zhang, Q.; Liu, R.; Qiu, B.; Rasool, M.; Liu, Z.; Meng, J.-Q.; Sun, L.-D.; Yan, C.-H.; Muller-Buschbaum, P.; Cheng, Y.-J. Green Facile Scalable Synthesis of Titania/Carbon Nanocomposites: New Use of Old Dental Resins. *ACS Appl. Mater. Interfaces* **2014**, *6*, 18461−18468.

(53) Cheng, Y.-J.; Antonucci, J. M.; Hudson, S. D.; Lin, N. J.; Zhang, X.; Lin-Gibson, S. Controlled In Situ Nanocavitation in Polymeric Materials. *Adv. Mater.* **2011**, *23* (3), 409−413.
(54) Xue, J. S.; Myrtle, K.; Dahn, J. R. An EpoxySilane Approach to Prepare Anode Materials for Rechargeable Lithium Ion Batteries. *J. Electrochem. Soc.* **1995**, *142* (9), 2927−2935.
(55) Tuinstra, F.; Koenig, J. L. Raman Spectrum of Graphite. *J. Chem. Phys.* **1970**, *53* (3), 1126−1130.
(56) Ferrari, A. C.; Robertson, J. Interpretation of Raman Spectra of Disordered and Amorphous Carbon. *Phys. Rev. B: Condens. Matter Mater. Phys.* **2000**, *61* (20), 14095−14107.
(57) Karakuscu, A.; Guider, R.; Pavesi, L.; Sorarù, G. D. White Luminescence from Sol-Gel-Derived SiOC Thin Films. *J. Am. Ceram. Soc.* **2009**, *92* (12), 2969−2974.
(58) Bujalski, D. R.; Grigoras, S.; Lee, W. L. N.; Wieber, G. M.; Zank, G. A. Stoichiometry Control of SiOC Ceramics by Siloxane Polymer Functionality. *J. Mater. Chem.* **1998**, *8* (6), 1427−1433.

chinaXiv:201705.00533v1